Controlled Resonant Magnetic Perturbation Physics Studies on EXTRAP T2R

L. Frassinetti, K.E.J. Olofsson, M.W.M. Khan, P.R. Brunsell and J.R. Drake*
Association Euratom-VR, Alfvén Laboratory, Royal Inst. of Technology KTH, Stockholm

E-mail contact of main author: lorenzo.frassinetti@ee.kth.se

Abstract. The EXTRAP T2R feedback system is used to study and develop new tools for an advanced control of the MHD instabilities in fusion plasmas. New algorithms that allow a flexible control of each magnetic field harmonic at the plasma boundary and enables controlled RMP generation are described. The algorithms will then be used to study the RMP effect on the tearing mode dynamics and on the plasma flow. It will be shown that the RMP can induce oscillations in the TM amplitude and phase jumps and that the TM braking is complex phenomenon and not a simple velocity slowing down.

1. Introduction

External magnetic perturbations are now an essential tool in fusion plasma physics to address severe problems related to edge localized modes (ELMs), magnetic islands and neoclassical tearing modes (NTMs). Resonant magnetic perturbations (RMPs), by interacting with the corresponding plasma TM, can (i) produce stochastic magnetic field in the pedestal region mitigating ELMs [1], (ii) induce rotation for NTM-stabilization or (iii) move the magnetic island to an optimal position for ECCD stabilization [2]. External magnetic perturbations are also a useful tool for neoclassical toroidal viscosity studies. While theoretical studies on the interaction between RMPs and TMs are relatively developed, from an experimental point of view, the effect of an RMP on the TM dynamics and on the plasma flow is not yet studied in a controlled fashion.

The EXTRAP T2R feedback systemis used to control the magnetic boundary [3]. Common feedback techniques are the intelligent shell (IS) [4] and the more advanced mode control (MC) [5]. New algorithms allowing a flexible control of each harmonic and enabling controlled RMP generation have been recently tested on EXTRAP-T2R [6].

The present work describes the contribution of the EXTRAP T2R reversed-field pinch (RFP) to the study of the RMP effect on the TM dynamics and on the plasma flow. The paper is organized as follows. Section 2 describes the new algorithms for mode control and their experimental implementation. The physics studies of the RMP effect on EXTRAP T2R plasma are discussed in Section 3. Conclusions are presented in section 4.

2. Advanced feedback algorithms for MHD studies in EXTRAP T2R

EXTRAP T2R and its feedback hardware are described in Section 2.1. Section 2.2 describes an improvement of the IS algorithm, the “revised” intelligent shell (RIS). Section 2.3 describes an algorithm that can be considered as a generalization of the clean mode control (CMC) [7], the fast fourier transform (FFT)-decoupled control system.

2.1. EXTRAP T2R and its feedback system

EXTRAP T2R is a reversed-field pinch machine with major radius 1.24m and minor radius 0.183m [8]. Typical plasmas are characterized by current ~100kA, electron temperature 300-400eV and plasma density $\sim 10^{19}$ m^{-3}.

The vacuum vessel is located at r_v=0.192 m and has a time constant $\tau_v \approx 0.28$ ms for the mode $(m, n) = (1, -12)$. The shell, located outside the vacuum vessel at r_w=0.198m, has a

nominal long shell time constant $\tau_w \approx 13.8$ ms. Typical discharge duration is between 70 and 90 ms.
The EXTRAP T2R feedback system includes power amplifiers, active coils, sensor coils, and the digital controller. Power amplifiers and active coils will be hereafter called "actuators". The active saddle coils are placed outside the shell at the minor radius r_a=0.238m and cover the shell surface with M_a = 4 loops in the poloidal direction and N_a =32 loops in the toroidal direction. The nominal angular extent of the active coil is $\Delta\theta_a = 360^\circ/M_a$ and $\Delta\phi_a = 360^\circ/N_a = 11.25^\circ$. The sensor coils are a subset of a magnetic diagnostic flux loop array and resolve the radial magnetic field component of m=1 modes $b^r_{1,n}$ with a toroidal resolution up to $|n|$ =16. They are located between the vessel and the shell at r_s=0.197m. The array covers the shell surface with M_s = 4 loops and N_s = 64 loops. The angular extent of the sensors is $\Delta\theta_s = 360\circ/M_s$ and $\Delta\phi_s = 360\circ/N_s = 5.625\circ$ in the poloidal and toroidal directions, respectively. Only the 4 × 32 loops located at the active coil positions are used in the feedback algorithm. At each toroidal position, active coils and sensor coils are m = 1 pair-connected.

2.2. The revised intelligent shell (RIS)

The intelligent shell (IS) concept was initially proposed by Bishop [4]. The basic idea is that the active coil i must respond to the radial magnetic field b^r_i measured by the corresponding sensor coil. If v_i is the input voltage to the actuator i, the IS feedback law can be written as:

$$v_i = -F_{PID}(s) b_i^r \qquad (1)$$

where F_{PID} is the PID transfer matrix i.e. a diagonal matrix that contains the proportional, integral and derivative (PID) gains. Ideally, the final result of the IS feedback would be to obtain zero radial magnetic field at the sensor coils in order to simulate a perfect conductor surface. Indeed, the IS has proven to be a useful tool for resistive wall mode (RWM) stabilization in several machines [9,10].
In this work, the IS concept is treated in a generalized way by enabling *output-tracking*. With the output-tracking capability, the user can decide a reference signal (to be compared with the sensor signals) for each harmonic individually (time-dependent amplitude and phase). The feedback will control the magnetic boundary to produce the reference signal at the sensors. If all reference signals are zero then the same effect of a standard IS is obtained. If the reference signal of a resonant harmonic is non-zero, then an RMP is generated. The schematic for the realization of the RIS feedback is shown in figure 1. It is composed of three main parts: (i) the actuators (power amplifiers and active coils) that produce a coil current $I_i(t)$, (II) the plant, i.e. the machine with its passive structures (vacuum vessel and resistive shell), the sensor coils and the plasma, (III) the digital controller that determines the feedback law and calculates the voltage input $v_i(t)$ to the actuators. This is a typical multiple-input-multiple-output (MIMO) system in the sense that the multiple coil currents $I_i(t)$ are the input to the machine plant and the sensor coils measurements $b_i^r(t)$ are the output.

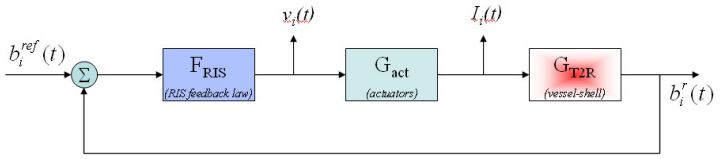

Figure 1: Model for RIS feedback

To formalize the above described MIMO model, the state-space formalism is used [6]:

$$\begin{cases} \dot{\mathbf{w}} = A\mathbf{w} + B\mathbf{I} \\ \mathbf{b}^r = C\mathbf{w} \end{cases} \quad (2)$$

where **I** is a vector containing all the actuators currents $I_i(t)$, $\mathbf{b}^r$ is a vector containing the sensor coil measurements $b_i^r(t)$ and the dot represents the time derivative. The variable **w** is the state of the system and does not require any strict interpretation; for sake of the reader it might be identified with the radial magnetic field. Finally, the matrices A, B and C are determined during the procedure of plant identification. Equations (2) are particularly simple if rewritten in the Laplace space (remember that $\mathcal{L}\dot{x}(t) = sx(s)$ where $\mathcal{L}$ represents the Laplace transform):

$$\mathbf{b}^r = G_{T2R}(s)\mathbf{I} \quad (3)$$

where G_{T2R} is the transfer matrix of the system: $G_{T2R}=C(sJ-A)^{-1}B$ and J is the identity matrix. The currents **I** depend on the input voltages $v_i(t)$ through:

$$\mathbf{I} = G_{act}(s)\mathbf{v} \quad (4)$$

where **v** is the vector containing the $v_i(t)$ and G_{act} is a matrix representing actuator dynamics. To "close the loop" and have a feedback control on $\mathbf{b}^r$, a feedback algorithm is needed to relate the output $\mathbf{b}^r$ of the system to the input voltages **v**. The feedback law used is the following:

$$\mathbf{v} = F_{RIS}(s)(\mathbf{b}^{ref} - \mathbf{b}^r) \quad (5)$$

where $F_{RIS}=M_{eq}F_{PID}$ with F_{PID} a diagonal matrix containing the PID gains and M_{eq} a tridiagonal matrix aiming to equalize the transfer channels. An important characteristic of the feedback law (5) is that it works in the real space, using the direct measurements of the sensor coils b_i^r and directly determining the input voltage to each actuators v_i.

To implement the RIS algorithm, the identification of the matrices G_{act}, G_{T2R} and F_{RIS}, is necessary. Here only the main logic steps are presented, for details see reference [6].

The identification of the matrix G_{act} can be considered as a calibration of the actuators: given an input signal to a power amplifier it is necessary to know the corresponding coil current produced. From a practical point of view, an analytic expression dependent on free parameters is obtained for G_{act} by modeling the actuators as a system composed of a low pass filter, a high pass filter, a delay (τ_h) and a static gain. The free parameters are calculated by measuring the coil current produced by using input voltages perturbed with a pseudo-random-binary-sequence (PRBS) and then comparing experimental results with the model.

The identification of the matrix G_{T2R} can be considered as a calibration of the machine passive structures (shell, vessel, sensor coils and other mechanical structures): given the coil current **I** in the actuators, we need to know the signal measured by the coil *j*: $b_j^r = \sum_{i=1}^{N} G_{T2R}^{i,j} I_i$. Note that this formulation takes into consideration the fact that the field measured by the coil *j* is affected by the coil current produced by all the actuators. Like for the actuator identification, an analytic expression for $G_{T2R}(s)$ is obtained and the free parameters are determined by applying the PRBS method to vacuum shots.

The tuning of the feedback law, i.e. the identification of the matrix $F_{RIS}(s)$, consists in the determination of the two matrices M_{eq} and F_{PID}. M_{eq} equalizes the transfer channels: ideally, a current induced only in the active coil *i* should produce a signal only in the corresponding sensor coil *i*. M_{eq} is needed to induce currents in the neighbor active coils

in order that total measured field in the neighbor sensors is close to zero. Details on the determination of M_{eq} can be found in [6]. F_{PID} is a diagonal matrix containing the PID gains for each channel. The gains are determined with a rule of thumb i.e. by comparing the EXTRAP T2R model with a second order unstable process for which the optimal gains are known.

This last step implies the assignment of a nominal instability γ=+1, which means that the PID controller assumes that local response of the b_i^r diffusion is unstable on the order of the local diffusion time.

The RIS algorithm is developed using two main assumptions: (i) the system identification performed in vacuum shots is valid also in plasma shots and (ii) the PID tuning is performed using a nominal instability γ=+1 (i.e. no information on the plasma dynamics). An experimental application of the RIS is shown in figure 2. Figure 2(a) shows the time evolution the radial component of the magnetic field harmonics as measured by the sensor coils for a shot without feedback and figure 2(b) with the standard IS. Figure 2(c) shows the $b^r_{m,n}$ evolution for a shot with RIS and reference signals set to zero for all harmonics. The IS and the RIS have similar effects. Figures 3(a) and 3(b) show $b^r_{m,n}$ for a RIS shot with reference signal $b^{ref}_{1,-12}=0.4mT$. The presence of the external perturbation does not affect the length of the discharge nor the suppression level of the other harmonics. Figures 3(c) and 3(d) show the coil current harmonic $I_{1,n}$ induced to generate the magnetic field shown in figure 3(a). The determination, by the controller, of the required harmonics produced by the active coils is clearly not trivial.

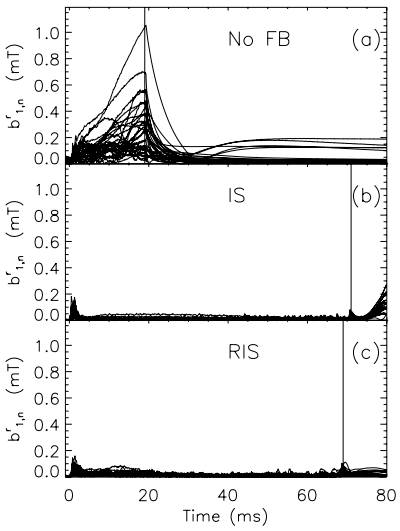

Figure 2: m=1 radial magnetic field harmonics for a plasma (a) without feedback, (b) with IS and (c) with RIS.

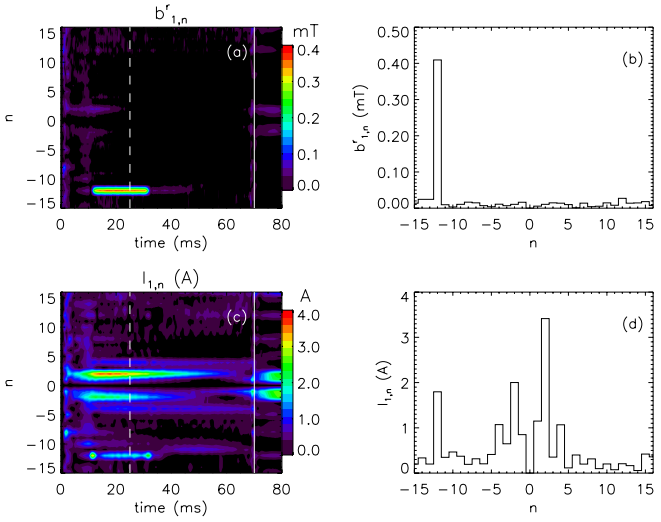

Figure 3: (a) m=1 radial magnetic field harmonics for a plasma with RIS and reference signal $b^{ref}_{1,-12}=0.4mT$. (b) Corresponding spectrum at t=25ms. (c) Evolution of corresponding active coil current harmonics and (d) spectrum at t=25ms. The vertical continuous lines in frames (a) and (c) highlight the end of the discharge.

2.3. The FFT decoupled control system

The RIS feedback has very good capability but its algorithm has non-optimal characteristics. The control is not tuned on the experimental plasma response but a general "nominal instability" γ=+1 is assumed. And the RIS feedback, working in the real space, cannot solve the m=1 aliasing problem originated by the finite number of sensor and active coils. The feedback described in this section tries to solve both these issues by

working in the mode space:

$$\mathbf{v} = M_{eq} W_{DFT}^{-1} F_{dec}(s)(L\mathbf{b}_f^{ref} + \mathbf{b}_f^r) \qquad (6)$$

where the subscript f denotes the spatial discrete Fourier transform (DFT), $\mathbf{b}_f^r = W_{DFT}\mathbf{b}^r$ with the matrix W_{DFT} that operates as the linear FFT. A detailed description can be found in [11]. $\mathbf{b}_f^r$ is a vector containing all the harmonics measured by the sensor coils and $\mathbf{b}_f^{ref}$ is a vector with the reference signals defined in the mode-space. F_{dec} is a diagonal controller matrix and L a diagonal constant matrix. Equation 6 is the feedback law used in the new algorithm.

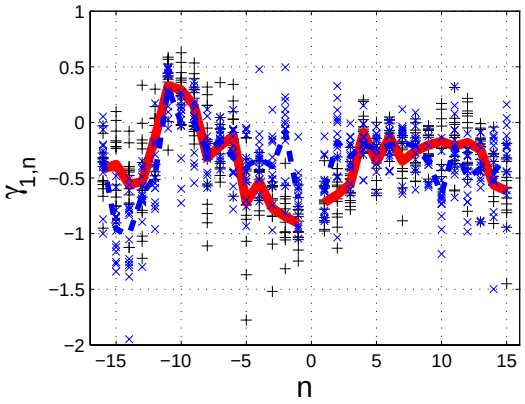

Figure 4. Growth rate determined with the closed loop identification experiments.

To solve the aliasing problem, the system inputs and outputs are considered in the mode space so that the new transfer matrix can be written as $b^r_{m,n}=G_{m,n}I_{m,n}$, where: $G_{m,n} = \sum_{m',n'} G_{m',n'}$ with m'=1,3,5 and n'=n,n-32,n+32. The matrix $G_{m',n'}$ can be calculate by discretizing the equation that describes the resistive wall mode (RWM) dynamic, $\tau_{m,n}\dot{b}^r_{m,n} - \hat{\gamma}_{m,n} b^r_{m,n} = b^{ext}_{m,n}$ [12], in order to obtain an analytic expression: $G_{m',n'}(s) = G_{m',n'}(\hat{\gamma}_{m',n'}, \tau_{m',n'}, p_{m',n'}, s)$ where, $\gamma_{m,n}$ is the normalized growth rate, $\tau_{m,n}$ is the diffusion time through a passive shell, $p_{m,n}$ are parameters dependent on the machine geometry and $b^{ext}_{m,n}$ is the external perturbation. The identification of the plasma parameters is done by applying the PRBS method to plasma shots and the results for the growth rates are plotted in figure 4.

External plasma response ($\gamma_{m,n}$, $\tau_{m,n}$ and $p_{m,n}$) and actuator response (section 2.2) are now available. The final step is to determine the controller matrix F_{DEC}. The equations of system in the mode space can be written as:

$$\begin{cases} \dot{\mathbf{w}} = A\mathbf{w} + B\,\mathrm{I}_{m,n} + Ne^1_{m,n} \\ b^r_{m,n} = C\mathbf{w} + e^2_{m,n} \\ b^1_{m,n} = M\mathbf{w} \end{cases} \qquad (7)$$

	$\langle b^r_{m=1} \rangle$ (mT)	$\langle b^r_{m=1} \rangle$ (%)	$\langle I^{coil}_{m=1} \rangle$ (A)
No Feedback	0.17±0.1	100	-
IS	0.008±0.004	4±2	8±3
RIS	0.008±0.004	4±2	5±2
FFT DEC (IS-like)	0.006±0.003	3±2	5±2
FFT DEC (CMC-like)	0.006±0.003	3±2	5±2

Table 1. Comparison of the algorithm performances.

where $e^1_{m,n}$ and $e^2_{m,n}$ are the applied and the measured error field respectively. Respect to equation 2, the model has the new term $b^1_{m,n}=M\mathbf{w}$ which represents the part of the output $b^r_{m,n}$ purely due to the m=1 mode i.e. without the aliasing. The controller matrix F_{DEC} is determined in order to minimize the variance of the output signal [13]. By considering the variance of $b^r_{m,n}$ a normal RIS is obtained. The minimization of $b^1_{m,n}$ variance gives a CMC feedback. To include the output tracking, $b^r_{m,n}$ is substituted with $b^r_{m,n} + lb^{ref}_{m,n}$.

A comparison of the performances of the different algorithms is shown in table 1. The figure of merit used is $\langle x_{m=1} \rangle = (\Sigma_{n=-16,15} \langle x_{1,n} \rangle_t)/32$ where $\langle x_{1,n} \rangle_t$ is the time average between 10ms to the end of the discharge. When the IS is applied, the measured $\langle b^r_{m=1} \rangle$ is 4% the measured field when no feedback is applied. The RIS has similar performances, but since

the algorithm is optimized to the EXTRAP T2R plant, a lower coil current is needed. With the FFT decoupled algorithm, $\langle b^r_{m=1} \rangle$ can be reduced to 3%.

3. RMP effect on plasma dynamics

The above described algorithms provide a useful tool to generate RMPs and to study their effect on the dynamics of the tearing modes (TM) and on the plasma flow. In EXTRAP T2R, the most internal TM corresponds to the helicity *(m,n)=(1,-12)* and it is characterized by a helical angular velocity in the range ω≈20-40krad/s, in agreement with plasma flow measurements [14].

3.1. Effect on TM dynamics

The typical TM dynamics in EXTRAP T2R is characterized by sawtooth crashes (relaxation events) that occur with a period around 0.3-0.4ms. When no external perturbation is present, the TM amplitude is relatively steady in between crashes and the TM velocity has no significant variations [15]. The application of an external perturbation can drastically affect this behavior. In figure 5(a) the time evolution of the most internal TM (m=1, n=-12) is shown when an RMP with amplitude 0.3mT and same helicity is applied. A relatively clear sinusoidal modulation is present. This modulation is well related to the mode phase. Figure 5(b) shows the correlation between the TM amplitude and the phase difference $\Delta\phi$ between the TM and the applied RMP. Approximately, amplitude amplification occurs when the TM is in phase with the RMP and amplitude suppression when the TM is out of phase. A similar correlation is found for the TM velocity, but acceleration and deceleration phases have a π/2 shift respect to the TM amplitude amplification and suppression.

This behavior is in good agreement with the model described in reference [16]. According to the model, the RMP modifies the Rutherford equation by adding a perturbation proportional to: $\dot{b}^{TM}_{m,n} \approx k_1 b^{RMP}_{m,n} \cos\Delta\phi$ and modifies the torque balance equation with a perturbation proportional to $\Delta\dot{\omega}^{TM}_{m,n} \approx k_2 b^{RMP}_{m,n} b^{TM}_{m,n} \sin\Delta\phi$, where $\Delta\dot{\omega}^{TM}_{m,n}$ is the time derivative of the angular velocity variation and k_1, k_2 are constants dependent on the geometry and on the viscosity. A simulation obtained by adapting the model to EXTRAP T2R geometry and equilibrium gives a reasonable agreement with the experimental results, figure

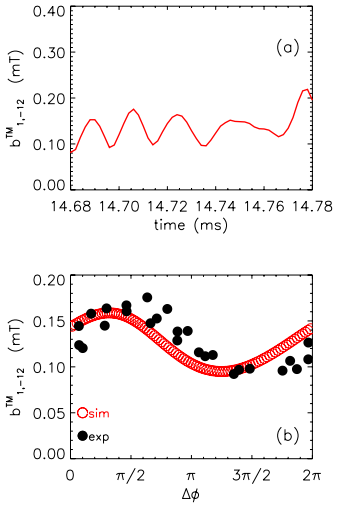

Figure 5. (a) TM amplitude evolution with applied RMP $b^r_{1,-12}$=0.3mT. (b) TM amplitude vs phase difference for experimental data (full dots) and modeled data (open dots).

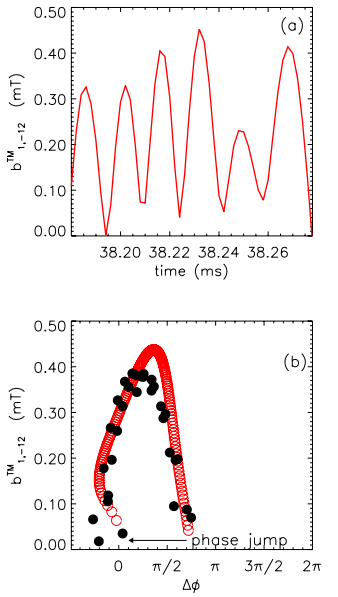

Figure 6. (a) TM amplitude time evolution when a 0.5mT RMP with helicity (1,-12) is applied. (b) Correlation between TM amplitude and phase difference for experimental data (full dots) and modeled data (open dots).

5(b). The shift between modeled and experimental data is probably due to a non precise estimation of the shell time constant.

A significantly different TM dynamics is obtained when the RMP amplitude is relatively large. In figure 6(a) we show the TM amplitude time evolution when and the external perturbation $b_{1,-12}^{RMP} = 0.5mT$ is applied. In this case the modulation is much stronger and when TM and RMP are out of phase the TM amplitude can be suppressed to zero. After the suppression, the TM has a π phase flip and re-appears approximately in phase with the RMP, see figure 6(b). A reasonable agreement between model and experiment is found.

Finally, it is worth mentioning that the two dynamics above described can occur during the same sawtooth cycle. For example, the dynamics characterized by the weak TM amplitude oscillation can be followed by the phase jumps and eventually by the TM wall locking [15].

3.2. Effect on plasma flow and on TM velocity

The RMP produces a perturbation on the TM velocity. The perturbation is approximately dependent on the phase difference between TM and RMP: $\Delta\omega_{m,n}^{TM} \propto \cos\Delta\phi(t)$, and the therefore the velocity is characterized by phases of acceleration and deceleration, see figure 7(a). Due to the plasma viscosity and to the mode amplitude modulation the phase difference $\Delta\phi(t)$ is not linear in t and the TM spends more time in the deceleration phase than in the acceleration phase. Therefore, an overall TM braking effect is observed, see the continuous line in figure 7(b). Note the different time scales of the two phenomena: the velocity modulation occurs on the time scale $\tau_{fast}\approx 10\mu s$, while the velocity braking is much slower with a time scale $\tau_{slow}\approx 10ms$. In figure 7(b) the TM velocity has been smoothed with a 1ms window to remove the fast oscillations and highlight the braking.

Also the plasma flow is modified by the RMP application. In figure 7(b) the dots correspond to the toroidal velocity of OV as measured by the Doppler shift using a Czerny-Turner spectrometer. OV impurity is mainly concentrated in EXTRAP T2R plasma core and therefore (assuming that impurities and plasma co-rotate) its velocity is approximately representative of the plasma flow in the region where the (1,-12) TM is resonant. Since

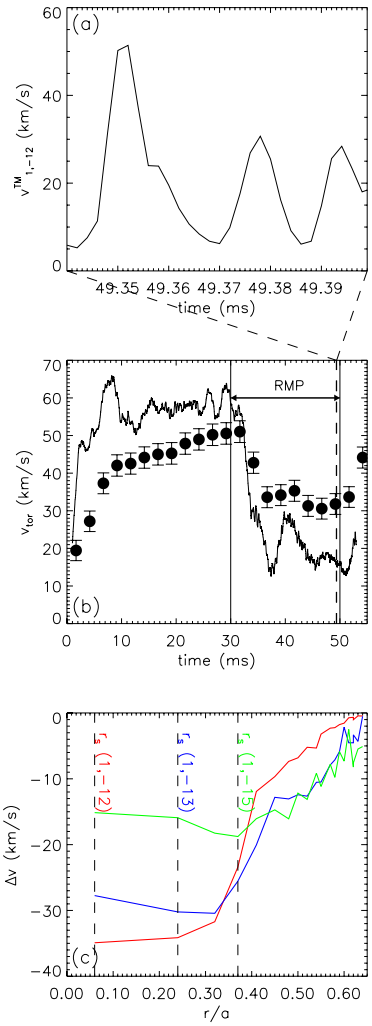

Figure 7. (a) TM velocity modulation on a short time scale when a 0.5mT RMP with helicity (1,-12) is applied. (b) TM velocity (continous line) and OV velocity (dots) on a long time scale. (c) TM velocity profile variation for three different shots. Red: RMP (1,-12) is applied; blue: RMP (1,-13) and green: RMP(1,-15).

the ion velocity is a line integrated measurement while the TM velocity can be considered as a local measurement, differences are unavoidable. Nevertheless, TM and OV impurity velocities show a reasonable agreement.
It is interesting to observe that the deceleration is not limited to the plasma core and that the whole velocity profile is affected. This result is obtained both by measuring the toroidal velocity of impurities concentrated not in the core and by analyzing the velocity of TMs that are not resonant in the core. Figure 7(c) shows the variation of TM velocity profile when an RMP is applied. The three lines correspond to three different shots. For the red line an RMP with helicity (1,-12) is applied, for the blue the helicity (1,-13) is used and for the green the helicity (1,-15). In all three cases the RMP amplitude is 0.3mT and the profiles are calculated when the TM velocity has reached a steady state. Despite the RMP amplitude is the same, the TM velocity variation is different both in the amplitude and in the profile shape: the maximum variation is obtained approximately at the resonant surface corresponding to the helicity of the applied RMP.

4. Conclusion

Two new feedback algorithms have been developed by exploiting modern control theory. In terms of used control current and/or mode suppression, both algorithms have better performances than the original IS concept. Moreover, they introduce the output tracking capability that is essential to perform physics studies of the RMP effect on the plasma.
RMPs have a significant effect both on the TM dynamic and on the plasma flow. RMPs can induce strong oscillations in the TM amplitude, phase jumps and TM velocity reduction. The TM braking is not a simple phenomenon and is characterized by a fast velocity oscillation that in a long time scale induces a velocity deceleration.

References

[1] Evans T.E. *et al.*, 2004 Phys. Rev. Lett. **92**, 235003.
[2] Maraschek M. *et al.*, 2007 Phys. Rev. Lett. **98**, 025005.
[3] Brunsell P.R. *et al.,* 2007 Phys. Plasmas **14**, 102505.
[4] Bishop C., 1989 Plasma Phys. Control. Fusion **31**, 1179.
[5] Paccagnella R. *et al.*, 2006 Phys. Rev. Lett. **97**, 075001.
[6] Olofsson K.E.J. and Brunsell P.R., 2009 Fus. Engr. and Design **84**, 1455.
[7] Zanca P. *et al.*, 2007 Nucl. Fusion **47,** 1425.
[8] Brunsell P. *et al.*, 2001, Plasma Phys. Control. Fusion **43**, 1457.
[9] Brunsell P. *et al.*, 2004, Phys. Rev. Lett. **93**, 225001.
[10] Martini S. *et al.*, 2007 Nucl. Fusion **47** 783.
[11] Fitzpatrick R. *et al.*, 1999 Phys. Plasmas **6** 3536.
[12] Olofsson E. et al. *,* 2010 Plasma Phys. Control. Fusion **52**, 104005.
[13] Olofsson E. et al. 2010, *IEEE Transactions on Plasma Science*, **38**, 365.
[14] Cecconello M. *et al.*, 2006, Plasma Phys. Control. Fusion **48**, 1311.
[15] Frassinetti L. *et al.*, 2010, Nucl. Fus. **50**, 035005.
[16] Fitzpatrick R. *et al.*, 2001 Phys. Plasmas **8** 4489.